Am J Physiol Cell Physiol 291: C757–C771, 2006.
First published May 10, 2006; doi:10.1152/ajpcell.00029.2006.

Cholesterol modulates the volume-regulated anion current in Ehrlich-Lettre ascites cells via effects on Rho and F-actin

Thomas Kjær Klausen, Charlotte Hougaard, Else K. Hoffmann, and Stine F. Pedersen

Department of Biochemistry, Institute of Molecular Biology and Physiology, University of Copenhagen, Copenhagen, Denmark

Submitted 24 January 2006; accepted in final form 6 May 2006

Klausen, Thomas Kjær, Charlotte Hougaard, Else K. Hoffmann, and Stine F. Pedersen. Cholesterol modulates the volume-regulated anion current in Ehrlich-Lettre ascites cells via effects on Rho and F-actin. *Am J Physiol Cell Physiol* 291: C757–C771, 2006. First published May 10, 2006; doi:10.1152/ajpcell.00029.2006.—The mechanisms controlling the volume-regulated anion current (VRAC) are incompletely elucidated. Here, we investigate the modulation of VRAC by cellular cholesterol and the potential involvement of F-actin, Rho, Rho kinase, and phosphatidylinositol-(4,5)-bisphosphate [PtdIns(4,5)P_2] in this process. In Ehrlich-Lettre ascites (ELA) cells, a current with biophysical and pharmacological properties characteristic of VRAC was activated by hypotonic swelling. A 44% increase in cellular cholesterol content had no detectable effects on F-actin organization or VRAC activity. A 47% reduction in cellular cholesterol content increased cortical and stress fiber-associated F-actin content in swollen cells. Cholesterol depletion increased VRAC activation rate and maximal current after a modest (15%), but not after a severe (36%) reduction in extracellular osmolarity. The cholesterol depletion-induced increase in maximal VRAC current was prevented by F-actin disruption using latrunculin B (LB), while the current activation rate was unaffected by LB, but dependent on Rho kinase. Rho activity was decreased by ~20% in modestly, and ~50% in severely swollen cells. In modestly swollen cells, this reduction was prevented by cholesterol depletion, which also increased isotonic Rho activity. Thrombin, which stimulates Rho and causes actin polymerization, potentiated VRAC in modestly swollen cells. VRAC activity was unaffected by inclusion of a water-soluble PtdIns(4,5)P_2 analogue or a PtdIns(4,5)P_2-blocking antibody in the pipette, or neomycin treatment to sequester PtdIns(4,5)P_2. It is suggested that in ELA cells, F-actin and Rho-Rho kinase modulate VRAC magnitude and activation rate, respectively, and that cholesterol depletion potentiates VRAC at least in part by preventing the hypotonicity-induced decrease in Rho activity and eliciting actin polymerization.

cell swelling; kinase; phospholipid phosphatidylinositol-(4,5)-bisphosphate; cytoskeleton

IN MOST CELL TYPES, volume regulation after cell swelling is dependent on the activation of separate conductive pathways for K^+ and Cl^- efflux (24). This was first proposed for Ehrlich ascites tumor (EAT) cells (23), in which the swelling activated anion current (VRAC) has been studied extensively (9, 52). The role of VRAC is, however, not limited to cell volume regulation after swelling, but includes regulation of, e.g., cell cycle progression, angiogenesis, and apoptotic cell death (40, 45). VRAC has been extensively characterized with respect to biophysical and pharmacological properties (40, 44), yet its molecular identity is unknown, and despite some progress in recent years (40), the mechanisms by which VRAC is regulated remain incompletely understood.

The early events elicited by cell swelling and resulting in VRAC activation have been proposed to include a reduction in intracellular ionic strength (56, 58, 66), and mechanical events such as membrane unfolding (23, 44, 49). In many cells including EAT cells, osmotic cell swelling is associated with a decrease in cellular F-actin content and/or disruption of cortical F-actin (20, 26, 29, 48, 50). The role of F-actin in regulation of VRAC has been studied in several cell types with varying conclusions (29, 35, 43, 70), possibly confounded by methodological issues regarding the use of cytochalasins to disrupt F-actin (for discussion, see Ref. 34).

Changes in membrane cholesterol content have been found to modulate the function of VRAC (30, 56) and other membrane transporters and channels (16, 19, 32, 56), as well as of numerous plasma membrane receptors (5). Cholesterol is a major component of the plasma membrane ordered microdomains known as lipid rafts and caveolae (4, 60), which play important roles in the control of signaling events, membrane ion transport, and membrane trafficking (59). Cholesterol depletion has been shown to disrupt the structure of rafts (4), including caveolae (67), and consequently, the effects of cholesterol on membrane protein function are frequently taken to indicate the involvement of rafts and/or caveolae. However, *1*) cholesterol is known to bind directly to membrane proteins, thereby regulating their function (17), and *2*) an increase in cholesterol content generally increases bilayer thickness (8), and stiffness (37), which modulate the "membrane deformation energy," a parameter dependent on bilayer thickness, mechanical properties, and monolayer equilibrium curvature, which has been used to describe the overall impact of these parameters on ion channel properties (25, 38). The membrane deformation energy contributes to the overall energy cost of channel opening/closing, as shown for, e.g., gramicidin channels and voltage-dependent Na^+ channels (31, 32).

In a cell (as opposed to a simple lipid vesicle), the effects of cholesterol on membrane deformability reflect both the phospholipid composition of the membrane and effects of cholesterol on cytoskeletal organization (see Ref. 69). Lipid rafts and caveolae interact with the actin cytoskeleton (22, 28, 36, 57, 61; see also Ref. 59), an interaction that may be disrupted by cholesterol depletion (21), and it appears that the effects of cholesterol content on membrane function are at least in some cases due to changes in the cellular distribution and content of F-actin (3, 6, 27).

Address for reprint requests and other correspondence: S. F. Pedersen, Dept. of Biochemistry, August Krogh Bldg., Institute for Molecular Biology and Physiology, Univ. of Copenhagen, 13 Universitetsparken, DK-2100 Copenhagen Ø, Denmark (e-mail: sfpedersen@aki.ku.dk).

The costs of publication of this article were defrayed in part by the payment of page charges. The article must therefore be hereby marked "*advertisement*" in accordance with 18 U.S.C. Section 1734 solely to indicate this fact.

Recent studies (30, 36) in bovine aortic endothelial (BAE) cells provided evidence that VRAC activity under modest osmotic gradients is increased by cholesterol depletion, an effect suggested to reflect changes in the cost of bilayer deformation and/or a (negative) regulation of VRAC by segregation to rafts/caveolae (30, 56). This, on the other hand, seems in contrast to the recent proposal that VRAC activation is dependent on the integrity of caveolae (63), and that caveolin-1 may increase VRAC availability in the plasma membrane and/or be involved in the signaling events leading to VRAC activation (64).

Small GTP binding (G) proteins of the Rho family are major regulators of F-actin polymerization (see Ref. 49) and have been implicated in the cytoskeletal reorganization elicited by cell volume perturbations (11, 13) as well as in the regulation or modulation of VRAC by cell swelling (7, 14, 42, 47). In vascular endothelial cells (7, 42) and NIH3T3 cells (47) the activity of the Rho-associated kinase (Rho kinase; ROK) is required for VRAC activation. RhoA and ROK associate with rafts and caveola and translocate to caveolae in an activation-dependent manner (62, 65), raising the possibility that the effect of cholesterol depletion on VRAC might involve changes in Rho kinase activity.

Similarly, the phospholipid phosphatidylinositol (4,5) bisphosphate [PtdIns(4,5)P_2], a major regulator of F-actin organization, has been shown to associate with lipid rafts (28, 57; see also Ref. 59), and loss or redistribution of membrane PtdIns(4,5)P_2 was proposed to underlie the complex F-actin reorganization in cholesterol-depleted human skin fibroblasts (27).

Thus the present study was initiated to determine the effects of cholesterol depletion and enrichment on isotonic and swelling-activated VRAC currents, and to investigate the involvement of the F-actin cytoskeleton, Rho, Rho kinase, and PtdIns(4,5)P_2 in the modulation of VRAC in ELA cells by cellular cholesterol content.

MATERIALS AND METHODS

Reagents. Unless otherwise stated, reagents were from Sigma-Aldrich (St. Louis, MO), Merck (Darmstadt, Germany), or Baker (Deventer, The Netherlands), and of the highest analytical grade. DIDS was dissolved at 50 mM and niflumic acid at 5 mM, both in DMSO. Stock solutions of Y27632 and latrunculin B (LB) (both from Calbiochem, Darmstadt, Germany) were prepared at 10 mM in ddH_2O and DMSO, respectively. The PtdIns(4,5)P_2 analog, PtdIns(4,5)P_2 dioctanoyl (Cayman, Ann Arbor, MI) was prepared as a 1 mM stock in chloroform:methanol:H_2O (3:2:1), aliquotted, and stored at −80°C until use. The monoclonal PtdIns(4,5)P_2 antibody was purchased from Assay Designs (Ann Arbor, MI). The antibody was diluted in PBS buffer containing 10% newborn calf serum and 0.05% NaN_2, and hence the corresponding control experiments were performed in the presence of this vehicle. In a third approach to modulating PtdIns(4,5)P_2 levels, PtdIns(4,5)P_2 was sequestered using neomycin (Sigma-Aldrich). Neomycin is an antibiotic which has previously been shown to bind PtdIns(4,5)P_2 (2) and inhibit the coupling between PtdIns(4,5)P_2 and the actin cytoskeleton (27, 28). Neomycin was dissolved at 10 mM in the normal growth medium, the pH of which was readjusted with NaOH, and the cells were incubated for 22–26 h in this medium before experiments.

Cell culture. The model system used was Ehrlich-Lettre ascites (ELA) cells, an adherent subtype of the EAT cells, in which VRAC is well characterized (52). ELA cells were grown in RPMI-1640 medium (Sigma-Aldrich) fortified with 10% fetal calf serum and 1% penicillin/streptomycin (Invitrogen, Carlsbad, CA) at 37°C and 5% CO_2. Cells were passaged every fourth day and used from *passages 5* to *30*.

Whole cell recording. For patch-clamp experiments, the cells were grown on coverslips in 40 mm petri dishes. Membrane currents were recorded from single ELA cells using the fast whole cell mode of the patch-clamp technique. The isotonic bath solution (300 mosmol/l) contained (in mM) 90 NaCl, 0 KCl, 1 $MgCl_2$, 1 $CaCl_2$, 10 HEPES, and 110 mannitol, pH 7.4 (pH adjusted with Tris in all solutions for electrophysiology). In the hypotonic bath solution, osmolarity was decreased to 255 and 190 mosmol/l by adjusting the amount of mannitol to 65 and 0 mM, respectively. Where indicated, Na^+ was replaced by *N*-methyl-D-glucamine ($NMDG^+$) in equimolar amounts in the extracellular solution. The intracellular pipette solution (295 mosmol/l) contained (in mM) 90 CsCl, 2 $MgCl_2$, 10 EGTA, 10 HEPES, 1.5 Na_2-ATP, 0.1 Na_2-GTP, and 80 mannitol, pH 7.4. For measurement of TRPM4 Ca^{2+} currents, two solutions were used. The bath solution was composed of 156 NaCl, 6 $CaCl_2$, 1 $MgCl_2$, 10 glucose, and 10 HEPES, and buffered at pH 7.4 with NaOH. The pipette solution was composed of 20 CsCl, 100 CsAsp, 1 $MgCl_2$, and 10 HEPES; pH 7.4 with NaOH. The osmolarity of solutions was routinely checked with the use of an osmometer (Knaur; Berlin, Germany).

Patch pipettes were pulled from borosilicate glass capillaries of 1.7 mm OD (Hounisens Laboratories, Riskov, Denmark) on a pipette puller (model pp-830; Narishige, Tokyo, Japan). The filled pipettes had resistances of 4.5–6.5 MΩ. A hydraulic micromanipulator (model WR-6, Narishige) was used for the positioning of pipettes and an Ag^-/AgCl wire served as the reference electrode. For anion selectivity studies, the reference electrode was 94 mM KCl in 3% agar.

Pipette offsets, series resistances (not >11 MΩ), and capacitive transients were compensated on the patch-clamp amplifier (model EPC7, List Electronic, Darmstadt, Germany). Currents were digitized with an analog-to-digital converter (model 1401+, Cambridge Electronic Design) at 500 Hz and filtered with the built-in four-pole Bessel filter at 3 kHz. Data acquisition and analysis were done with the Cambridge Electronic Design patch- and voltage-clamp software (version 6.41). The holding potential was −40 mV and voltage ramps from −80 to +80 mV and of 2.6-s duration were applied every 15 s, with a 500-ms prepulse at −80 mV preceding each ramp. Time-dependent kinetics were investigated by stepping the potential from −80 to +80 mV in 20 mV steps of 1 s, separated by 2-s intervals at the holding potential. Cells were continuously perfused at a rate of 2 ml/min with a complete exchange of the bath solution every 0.5 min. All anion channel experiments were performed at room temperature (18–21°C). However, because TRPM4 is not active at room temperature in ELA cells, these experiments were performed at 37°C by mounting recording chamber on a heated stage system (Broke).

Modulation and estimation of cellular cholesterol level. ELA cells were depleted of cholesterol by incubation with 5 mM methyl-β-cyclodextrin (MβCD) without cholesterol in RPMI-1640 medium for 1 h. Cholesterol-enriched ELA cells were prepared by incubation with 5 mM MβCD saturated with cholesterol (625 μM) for 3 h. The MβCD-cholesterol solution was prepared as previously described (10). To evaluate the cholesterol content, lipids were extracted from cell monolayers by incubating these for 30 min in isopropanol at room temperature, while lipid free cell content was subsequently solubilized in 1 M NaOH. This procedure quantitatively extracts all lipids (33). Extracted lipids were concentrated by partially evaporating isopropanol in purpose made apparatus, and cholesterol content was subsequently measured using the "cholesterol CHOD-PAP method" (Roche, Basel, Switzerland). This is a standard enzymatic reaction for spectrophotometric analysis, where the cholesterol content is linear to the absorbance at 500 nm. Cell protein was estimated from the lipid free NaOH solution using a BCA protein kit (Bio-Rad, Hercules, CA) with bovine serum albumin as a standard.

Neomycin pretreatment to sequester cellular PtdIns(4,5)P_2. PtdIns(4,5)P_2 was sequestered using neomycin (Sigma-Aldrich). Neomycin is an antibiotic which has previously been shown to bind PtdIns(4,5)P_2 (2) and inhibit the coupling between PtdIns(4,5)P_2 and the actin cytoskeleton (27, 28). Neomycin was dissolved at 10 mM in the normal growth medium, the pH of which was readjusted with NaOH, and the cells were incubated for 22–26 h in this medium before experiments.

Immunocytochemistry and confocal laser-scanning microscopy. For immunocytochemistry experiments, cells were grown to a confluence of 60–70% on no. 1 glass coverslips. Where indicated, cells were enriched or depleted of cholesterol as described above. For disruption of F-actin using LB, cells were incubated with LB (10 μM) for 1 h during the cholesterol depletion treatment. Before fixation, the cells were incubated for 2 min in either standard isotonic salt solution composed of (in mM) 143 NaCl, 5 KCl, 1 $MgSO_4$, 1 Na_2HPO_4, 1 $CaCl_2$, 3.3 MOPS, 3.3 TES, and 5 HEPES, or, where indicated, in the mannitol-containing isotonic solution used for electrophysiological experiments. The cells were fixed in 4% paraformaldehyde for 15 min on ice, permeabilized for 10 min in 0.1% Triton X-100, and blocked for 30 min in blocking buffer (PBS) composed of (in mM) 136.89 NaCl, 2.68 KCl, 8.1 Na_2HPO_4, and 1.47 KH_2PO_4 with 2% BSA. F-actin was stained with either FITC- or rhodamine-conjugated phalloidin (2 U/ml, Molecular Probes, Leiden, The Netherlands) in blocking buffer for 45 min at room temperature. The nuclei were stained with 4,6-diamidino-2-phenylindole (DAPI; 1:300, Molecular Probes) for 5 min in blocking buffer. After being stained, the cells were washed extensively in blocking buffer and mounted using *N*-propyl galleate mounting medium (Sigma-Aldrich). Confocal microcopy was performed using a Leica DM IRB/E microscope coupled to a confocal laser scanning unit (model TSC NT; Leica Lasertechnik, Heidelberg, Germany). Excitation of DAPI, FITC, and rhodamine was carried out using the 364 nm UV, and the 488 or 567 nm argon/krypton laser lines, respectively. Images were taken using a ×40/1.25 numerical aperture planapochromat objective, a 1.0 Airy disk pinhole, and an optical slice thickness of 1 μm. When multiple dyes were used, images were acquired by sequential scanning. Images (512 by 512 pixels) were frame averaged and presented in RGB pseudocolor.

Purification of Rho-GTP. Rho-GTP content was estimated using a commercial pull-down assay (Cytoskeleton, Denver, CO). Briefly, the cholesterol content of cells grown to 80% confluence in 10 cm petri dishes was modulated as described above, and cells were washed once with PBS and stimulated for 3 min with isotonic or hypotonic solution at room temperature. Cells were quickly washed in PBS, 500 μl of lysis binding buffer containing a protease inhibitor cocktail were added, cells were scraped off, and homogenates were transferred to Eppendorf tubes. Homogenates were cleared by centrifugation at 20,000 *g* for 5 min at 4°C. The cleared lysates (500 μl) were used for analysis of Rho-GTP content, and the remaining lysate for protein measurement and estimation of total Rho, as follows: 500 μl of cleared lysate were transferred to 20 μl of RBD purification bead solution, and 5 μl of protein inhibitor cocktail were added to the solution. Lysate and RBD beads were incubated at constant rotation for 1 h at 4°C. RBD beads were washed once with lysis binding buffer and once with washing buffer (5,000 *g*, 3 min, 4°C). RBD beads with bound Rho-GTP were spun down as above, the supernantant carefully removed, and the RBD bead pellet dissolved in 10 μl of NuPage LDS sample buffer (Invitrogen, Carlsbad, CA) containing 29% DTT and frozen at −80°C. Total Rho and purified Rho-GTP content were analyzed by SDS-PAGE and Western blot analysis as described below. For positive controls, the cells were transfected with Myc-tagged, constitutively active Rho (RhoQ63L, a kind gift from Dr. Andras Kapus, St. Michael's Hospital, Toronto, ONT, Canada), using Lipofectamine 2000 (Invitrogen), and 4 μg of DNA per 10 cm dish. Forty-eight hours after transfection, the cells were lysed and Rho-GTP isolated as described above.

SDS-PAGE and Western blot analysis. Total Rho and precipitated Rho-GTP protein samples were resolved by SDS-PAGE under denaturating and reducing conditions using 12% Bis-Tris gels with NuPage Mes SDS running buffer and an XCell system (model E19001; Novex, San Diego, CA). The protein concentration of cleared total cell lysates was estimated using a BCA protein kit (Bio-Rad) with BSA as standard. The amount of protein loaded per well was 20 μg for total Rho, and an amount corresponding to 0.74 mg of unpurified whole cell protein for purified Rho-GTP. Separated proteins were electrotransferred to Protran nitrocellulose membranes (Schleicher and Schuell, Keene, NH), membranes were stained with 1% Ponceau S Red solution (Sigma-Aldrich), blocked in 5% nonfat dry milk in 1× TBST (composed of 0.01 M Tris·HCl, pH 7.4, 0.15 M NaCl, and 0.1% Tween 20) for 75 min, incubated for 2 h with monoclonal anti-Rho antibody (Cytoskeleton) 1:500 in blocking buffer, washed extensively in TBST, and incubated for 1 h in with alkaline phophatase-conjugated goat-anti mouse antibody (Jackson ImmunoResearch, West Grove, PA), 1:500 in blocking buffer, all at room temperature. Membranes were washed extensively in TBST and developed using BCIP/NBT solution (Kirkegaard and Perry Laboratories, Gaithersburg, MD). Band intensity was evaluated by densitometric scanning using UN-SCAN-IT software (version 5.1, Silk Scientific, Orem, UT).

Data treatment and statistical analysis. Data are presented as means ± SE, with *n* denoting the number of cells tested. For comparison of data sets, Student's *t*-tests for paired and unpaired data were employed as appropriate. In patch-clamp experiments, the percent inhibition by DIDS and niflumic acid were calculated as

$$\%\ \text{inhibition} = \frac{I_{\text{control}} - I_{\text{drug}}}{I_{\text{control}}} 100\% \quad (1)$$

where I_{control} refers to the control current, and I_{drug} refers to the current measured in the presence of the drug. Permeability sequences were calculated from the experimentally determined V_{rev} shifts using the modified Goldman-Hodgkin-Katz equation as follows:

$$\frac{P_x}{P_{Cl}} = \frac{[Cl^-]_o \exp(-\Delta V_{\text{rev}} F/RT) - [Cl^-]_s}{[X^-]_o} \quad (2)$$

where P_x/P_{Cl} gives the relative permeability of the given anion (X) to Cl^-; $[Cl^-]_o$ is the Cl^- concentration in the standard bath solution, $[Cl^-]_s$ and $[X^-]_o$ are the concentrations of Cl^- and the substituting anion in the substituted medium, respectively, ΔV_{rev} is the measured shift in reversal potential, and F, R, and T have their usual meanings.

RESULTS

Characterization of swelling-activated Cl^- current in ELA cells. VRAC has not previously been characterized in ELA cells, and it was therefore important to first establish the biophysical and pharmacological characteristics of the current. Perfusion with hypotonic solution resulted in cell swelling (not shown) and development of a current which was readily reversible upon return to isotonic conditions, and which exhibited time-dependent inactivation and flat tail currents at depolarized potentials (Fig. 1*A*). The current was outwardly rectifying and the current magnitude was greater after exposure to a 36% hypotonic solution (190 mosmol/l) than to a 15% hypotonic solution (255 mosmol/l) (Fig. 1, *B–D*). The current V_{rev} was −12 ± 0.5 mV (n = 46) at 190 mosmol/l, compared with the calculated V_{rev} for Cl^- at 0 mV under these conditions. To investigate the possible contamination by cation currents, several experiments were performed, in which all extracellular Na^+ was substituted by $NMDG^+$. This resulted in a small shift in V_{rev} (−13.61 ± 0.63 mV to −15.01 ± 0.47

mV, $n = 7$, $P < 0.01$). However, returning to NaCl solution did not cause the reciprocal change in V_{rev} (-14.46 ± 1.04 mV, $n = 7$; $P > 0.5$), indicating that the shift in V_{rev} was not due to cation current modulation. Instead, as discussed in Ref. 53, this deviation from the theoretical value is likely to reflect a dilution of the intracellular solution, arising because the osmotic water inflow into Ehrlich cells is faster than the solution exchange via the patch pipette. From the Nernst equation, it may be calculated that the discrepancy between the calculated and experimental V_{rev} corresponds to a 38% dilution of the intracellular solution in the 190 mosmol/l bath solution. In the 15% hypotonic solution, V_{rev} was -5.63 ± 0.95 mV

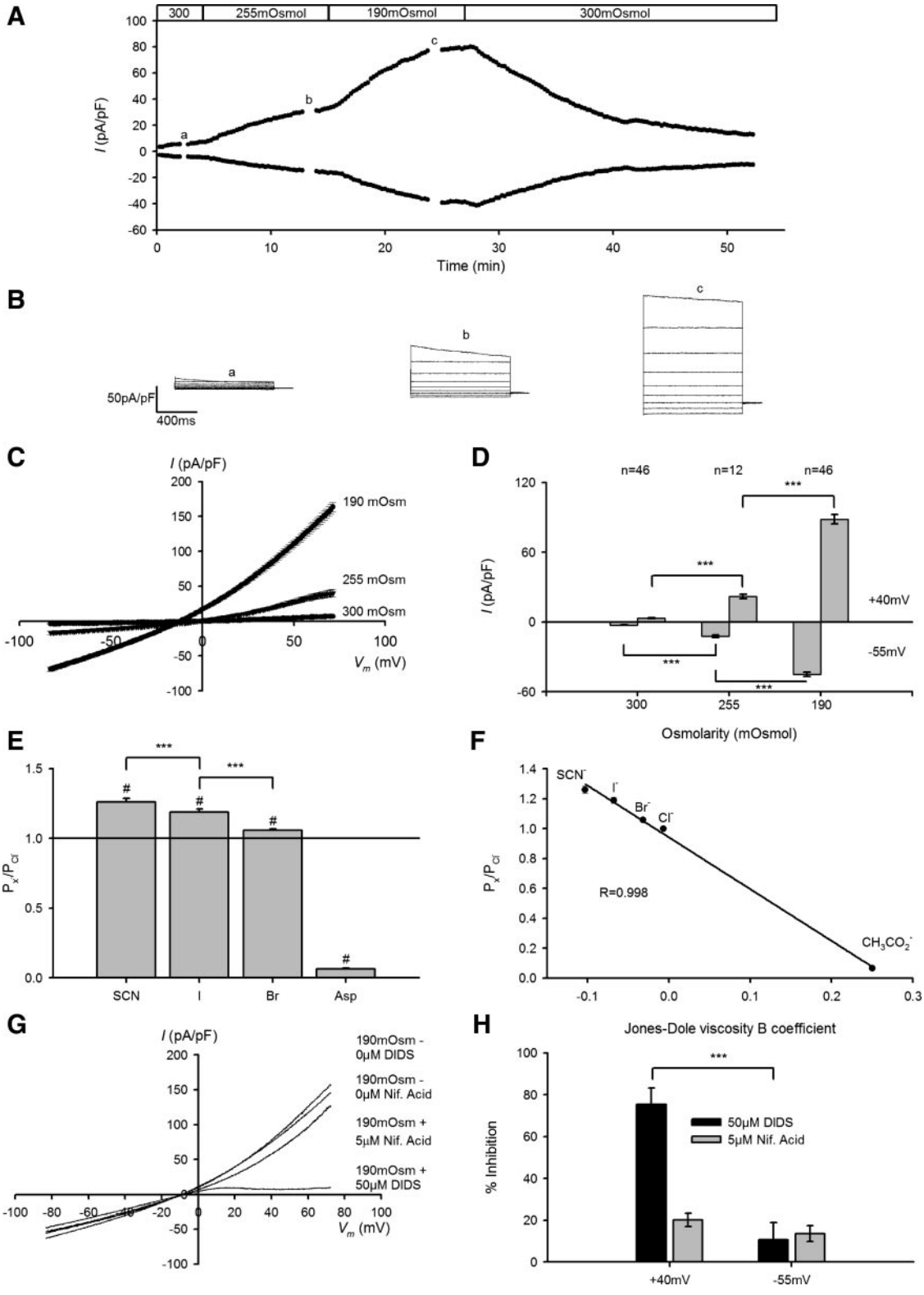

($n = 4$) in the presence, and -9.78 ± 1.07 ($n = 4$, $P < 0.05$) in the absence of Na^+. Because this shift was reversible when the cells were reexposed to the Na^+-containing bath solution, this indicates that a cation current is responsible for a minor fraction of the current measured in the standard hypotonic solution. The relative permeabilities of the current to various anions were estimated from the shifts in V_{rev} upon anion substitution, using the modified Goldman-Hodgkin-Katz equation (Fig. 1*E*). The anion permeability sequence obtained was the following: P_{SCN}: P_I: P_{Br}: P_{Cl}: P_{Asp} = 1.3 ± 0.03 ($n = 8$): 1.2 ± 0.02 ($n = 8$): 1.1 ± 0.01 ($n = 8$): 1: 0.06 ± 0.004 ($n = 4$), i.e., an Eisenman I permeation sequence. A linear correlation was noted between the relative permeability of the ion and the Jones-Dole viscosity B coefficient, a measure of ion-water interactions (Fig. 1*F*; see also DISCUSSION). Finally, application of DIDS (50 μM) inhibited the current in a voltage-dependent manner, with 75% and 11% inhibition at +40 mV and −55 mV, respectively, whereas inhibition by another Cl^- channel inhibitor, niflumic acid (5 μM), was small and voltage-independent, calculated at ~20% and 14%, respectively, at +40 and −55 mV (Fig. 1, *G* and *H*). Thus the swelling-activated Cl^- current in ELA cells exhibits characteristics similar to those described for the swelling-activated anion current, VRAC, in a wide range of cell types. Specifically, it may be noted that the only notable difference between the VRAC currents in ELA cells and the suspension cell line EAT cells, of which ELA cells are an adherent subtype, is that the degree of voltage-dependent inactivation in ELA cells observed in the present study was substantially lower than that in EAT cells (52).

Effects of cholesterol enrichment and depletion on activation of VRAC. The next series of experiments investigated the relationship between cellular cholesterol content, F-actin organization, and VRAC activity. Cellular cholesterol content was modified using MβCD in the absence or presence of added cholesterol (see MATERIALS AND METHODS). This resulted in a 47% increase, or a 44% decrease, respectively, in total cholesterol content in ELA cells (Fig. 2*A*).

Cholesterol enrichment had no effect on VRAC activation after either a 190 mosmol/l or a 255 mosmol/l hypotonic challenge (Fig. 2, *B* and C). In contrast, cholesterol depletion significantly potentiated VRAC after exposure to 255 mosmol/l of bath solution, but not after the more severe swelling in 190 mosmol/l solution (Fig. 2, *D* and *E*). The initial current activation rate, as calculated by linear regression to currents measured between 15 and 90 s after 255 mosmol/l hypotonic challenge was significantly increased in depleted cells. Thus an activation rate of 10.32 ± 1.86 pA pF^{-1} min^{-1} was found in depleted cells, whereas the rate was only 4.78 ± 0.78 pA pF^{-1} min^{-1} in control cells ($P < 0.05$).

As pointed out above, there was a small cation component in the current activated by 255 mosmol/l Na^+-containing bath solution. However, the shift in V_{rev} upon switching to 255 mosmol/l $NMDG^+$ solution was similar in depleted cells and control cells (−4.15 ± 1.30 mV and −3.17 ± 0.47, respectively, $n = 4$, $P = 0.51$), indicating that the cation permeability of cholesterol depleted cells is similar to that of control cells under these conditions, and hence that the augmenting effect of cholesterol depletion on the current measured in osmotically swollen cells is predominantly or exclusively an effect on VRAC.

We next investigated whether cholesterol depletion similarly activates VRAC in the absence of osmotic swelling. Under isotonic conditions, V_{rev} in both control ($n = 9$) and cholesterol depleted ($n = 7$) cells shifted significantly toward more negative values when Na^+ was replaced with $NMDG^+$, indicating a significant contribution from a cation current. Hence, characterization of the cholesterol sensitivity of the isotonic anion current was performed in both Na^+ and $NMDG^+$ bath solutions (Fig. 3). As shown, an outwardly rectifying current with time dependent inactivation at depolarized potentials, i.e., highly similar to VRAC, was active in both control and cholesterol depleted cells in NMDG Ringer (Fig. 3, *A–D*). Similar to the swelling-activated VRAC current, this current was significantly increased in depleted cells compared with control cells, indicating that cholesterol depletion partially activates VRAC under isotonic conditions. The cholesterol depletion-induced increase in isotonic current magnitude was, if anything ($P = 0.059$), greater in $NMDG^+$ than in Na^+ bath solution, substantiating the notion that the cholesterol depletion-sensitive current is carried by anions (Fig. 3, *E* and *F*).

Effects of cholesterol enrichment and depletion on F-actin organization. F-actin organization has been shown to be altered by changes in cellular cholesterol content, and has been implicated in swelling-induced VRAC activation (see *Introduction*). The effect of cholesterol enrichment and depletion on F-actin organization in ELA cells was assessed by confocal laser scanning microscopy of phalloidin-labeled cells (Fig. 4). As shown in Fig. 4*A*, neither cholesterol enrichment nor depletion had any detectable effect on cellular morphology. Images from the bottom, middle, and top of control cells (*images a–c*) illustrate the typical appearance of stress fibers and cortical F-actin in ELA cells. Cholesterol enrichment had no detectable effect on cellular F-actin organization and con-

Fig. 1. Characteristics of the swelling-activated anion current in Ehrlich-Lettre ascites (ELA) cells. From a holding potential of −40 mV, a prepulse of 500-ms duration was applied at −80 mV, followed by a voltage ramp from −80 to +80 mV. *A*: typical experiment showing the dose-dependent current activation as a function of time after hypotonic stimulation through the bath solution. The anion currents were measured at membrane potentials +40 and −55 mV at 300, 255, and 190 mosmol/l (shown as mOsm) as indicated. *B*: to investigate time dependent kinetics of the activated currents a step protocol from −80 to +80 mV with 20 mV steps was applied in the experiment shown in *A*, at the time points indicated by *a–c*. The duration of each step was 1 s, separated by 2 s at the holding potential of −40 mV (representative of 9 independent experiments). *C*: current-voltage (*I/V*) relationship for currents measured using the fast-ramp protocol, at 300 mosmol/l ($n = 46$), 255 mosmol/l ($n = 12$), and 190 mosmol/l ($n = 46$). *D*: summarized steady-state current density at −55 mV and +40 mV with an extracellular osmolarity of 190 mosmol/l ($n = 46$), 255 mosmol/l ($n = 12$), and 300 mosmol/l ($n = 46$). ***$P < 0.001$, vs. Student's *t*-test. *E*: anion selectivity of the activated current was investigated by analysis of shift in reversal potential (V_{rev}) after substitution of 79 mM extracellular Cl^- with SCN^- ($n = 8$), I^- ($n = 8$), Br^- ($n = 8$), and aspartate ($n = 4$). The figure depicts the summarized permeabilities relative to Cl^- as calculated from the modified GHK equation. #$P < 0.001$, V_{rev} for ion was significantly different from that for Cl^-. *F*: relative permeabilities from *E* were plotted as a function of the Jones-Dole viscosity B coefficient (see Refs. 12 and 54) of the indicated anions. For aspartate, the Jones-Dole viscosity B coefficient of the anionic sidechain is plotted. The straight line represents a linear fit. *G* and *H*: inhibitory effect of 50 μM DIDS and 5 μM niflumic acid on the current obtained in 190 mosmol/l bath solution. Inhibitory effects are calculated using *Eq. 2* (see MATERIALS AND METHODS). The data represent 3–5 independent experiments for each condition. ***$P < 0.001$, significant difference.

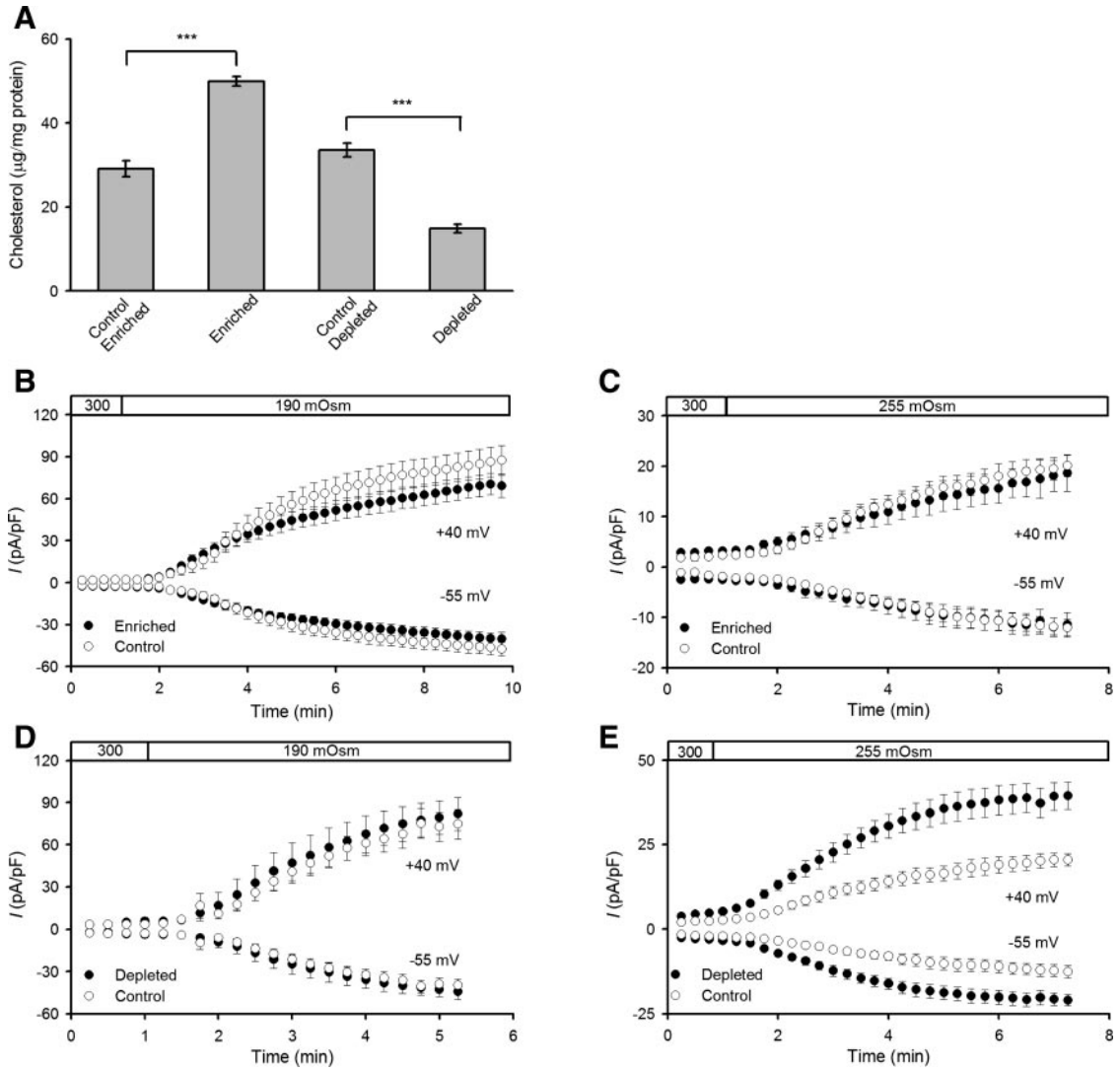

Fig. 2. Effect of cholesterol depletion and enrichment on the swelling-activated anion current in ELA cells. *A*: cellular cholesterol content was modulated using empty MβCD for depletion and cholesterol-loaded MβCD for enrichment, respectively, and measured by the CHOD-PAP method, as described in MATERIALS AND METHODS. The number of independent experiments were 6 (enrichment control), 6 (enrichment), 3 (depletion control), and 3 (depletion), respectively. *B* and *C*: cellular cholesterol content was increased as described in *A*, and current activation at −55 and +40 mV after exposure to 190 mosmol/l (*B*) or 255 mosmol/l (*C*) was measured using the fast ramp protocol described in legend to Fig. 1. *D* and *E*: cellular cholesterol content was reduced as described in *A*, and current activation at −55 and +40 mV after exposure to 190 mosmol/l (*D*) or 255 mosmol/l (*E*) was measured using the fast ramp protocol. The number of independent experiments were 6 (ctrl. for enrich. 255 mosmol/l), 5 (enrich. 255 mosmol/l), 9 (ctrl. for enrich. 190 mosmol/l), 9 (enrich. 190 mosmol/l), 6 (ctrl. for depl. 255 mosmol/l), 7 (depl. 255 mosmol/l), 6 (ctrl. for depl. 190 mosmol/l) and 6 (depl. 190 mosmol/l). ***$P < 0.001$, significant difference calculated by independent *t*-tests.

tent (*images g–i*). In contrast, cholesterol depletion was associated with a marked increase in F-actin labeling intensity, apparently both due to increased cortical F-actin polymerization and increased stress fiber formation (*images d–f*). Figure 4*B* shows the quantification of pixel intensities in the phalloidin-labeled cells, under isotonic and hypotonic conditions, in control cells and after cholesterol depletion and enrichment, respectively. As shown, in control cells both cytoplasmic (i.e., predominantly stress-fiber associated) and cortical F-actin levels were reduced by ~50% after 2 min of hypotonic swelling, consistent with previous findings in EAT cells (53). Under isotonic conditions, cholesterol depletion tended to increase cytoplasmic F-actin, although not quite significantly ($P = 0.11$), whereas cholesterol enrichment significantly decreased the cortical, but not the cytoplasmic, F-actin level. Cholesterol depletion abolished the decrease in F-actin seen in control cells under hypotonic conditions, and in fact resulted in a significant increase in F-actin levels compared with isotonic control conditions. In contrast, cholesterol enrichment had no effect on the swelling-induced decrease in F-actin levels. The images shown in Fig. 4 are obtained in cells exposed to mannitol-containing, low ionic strength isotonic saline as in the electrophysiology experiments, however, similar results were obtained in the standard isotonic saline ($n = 3$ and $n = 6$ for cholesterol enrichment and cholesterol depletion, respectively, data not shown).

Effects of LB on F-actin organization and VRAC activity. Pretreatment of ELA cells with LB, which reduces the cellular content of polymerized actin by sequestering actin monomers, lead to the essential disappearance of both F-actin stress fibers

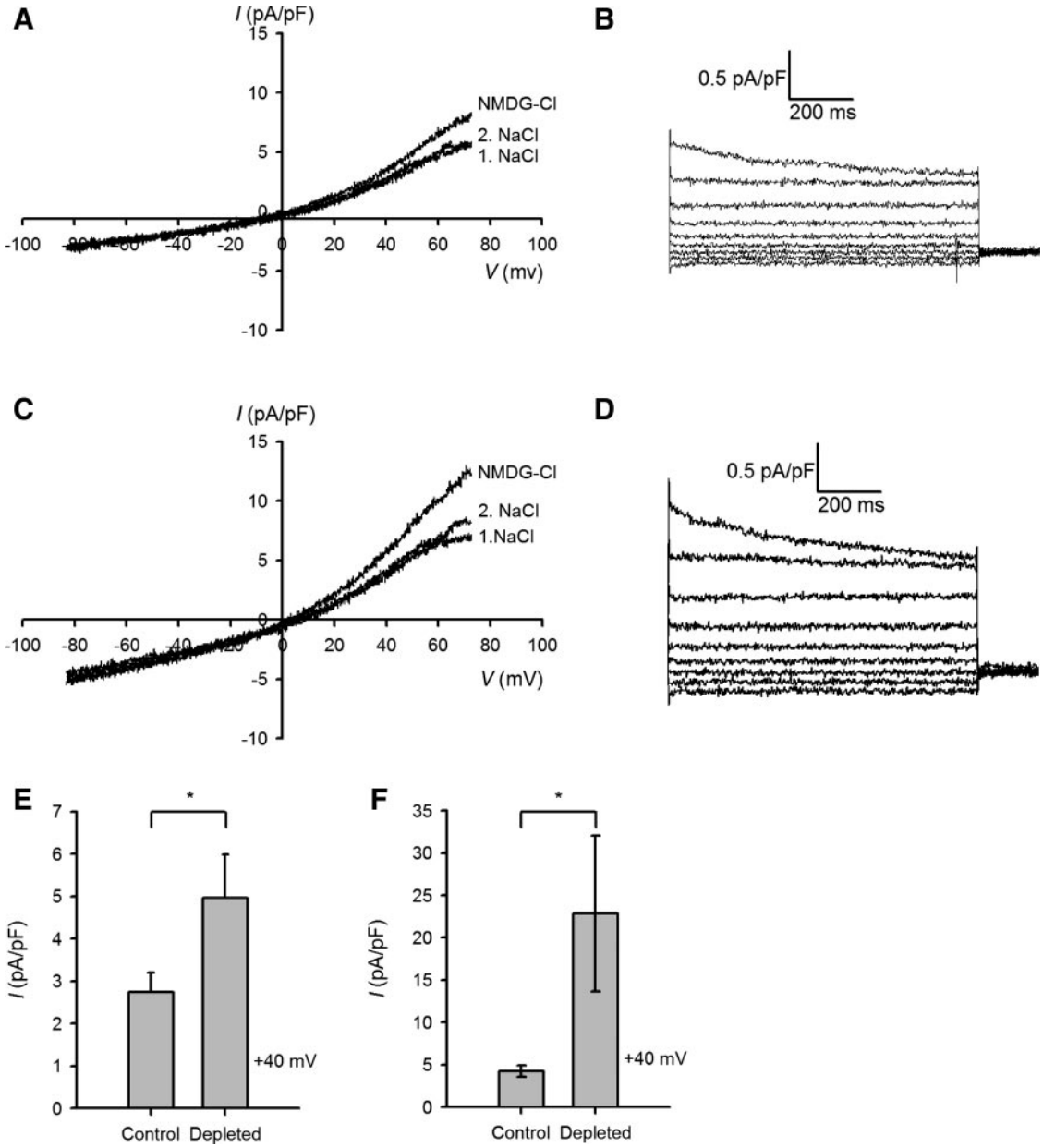

Fig. 3. Characterization of isotonic anion currents. Membrane cholesterol content was modulated as described in the legend to Fig. 2, and whole cell configuration was established using the standard NaCl bath solution (300 mosmol/l). Where indicated, NaCl was substituted by *N*-methyl-D-gluconate (NMDG)-Cl to exclude contributions from cation currents. This resulted in a significant change of V_{rev} from 5.46 ± 0.68 mV to 2.21 ± 0.73 mV in control cells ($n = 9$). V_{rev} after reexposure to NaCl solution was 4.05 ± 0.62 mV. In cholesterol depleted cells V_{rev} shifted from 3.61 ± 1.43 mV to −2.81 ± 0.94 mV upon shift from NaCl to NMDG-Cl bath solutions ($n = 7$) and to 4.73 ± 1.43 mV when reexposed to NaCl. *A* and *C*: representative *I/V* relationship for control and cholesterol depleted cells, respectively, measured using the fast voltage ramp protocol. "1. NaCl" and "2. NaCl" indicate the initial and re-exposure to NaCl solution, respectively. *B* and *D*: time- and voltage-dependent characteristics of the isotonic anion current measured in NMDG-Cl bath solution using the step protocol described in Fig. 1. *E* and *F*: mean current density measured in control and depleted cells at +40 mV in NaCl (*E*) and NMDG-Cl (*F*) bath solution, respectively. The number of independent experiments was 9 (ctrl.) and 7 (depl.). ***$P < 0.001$, significant difference at calculated by independent *t*-tests.

and cortical F-actin in the ELA cells (Fig. 5*A*). In control cells, LB treatment had no significant effect on VRAC under hypotonic (Fig. 5*B*) or isotonic (Fig. 5*F*) conditions. In cholesterol depleted cells, LB treatment reduced the hypotonic current magnitude to a value similar to that in undepleted control cells (Fig. 5*C*), whereas in contrast, the isotonic current in depleted cells was further potentiated by LB (Fig. 5*G*). Notably, the difference in activation rates between control and depleted cells was preserved despite the LB treatment. Thus activation rates of 1.86 ± 0.56 and 6.50 ± 1.18 pA pF^{-1} min^{-1} where observed in control and depleted cells, respectively ($P < 0.01$), yet the cholesterol depletion-induced increase in maximal VRAC current was abolished (Fig. 5*D*). The maximal swelling-induced VRAC currents are summarized in Fig. 5*E*.

The above data indicate that the cholesterol depletion-induced increase VRAC might be dependent on the increase in stress fiber content seen in the cholesterol depleted cells. Consistent with this notion, the serine protease thrombin,

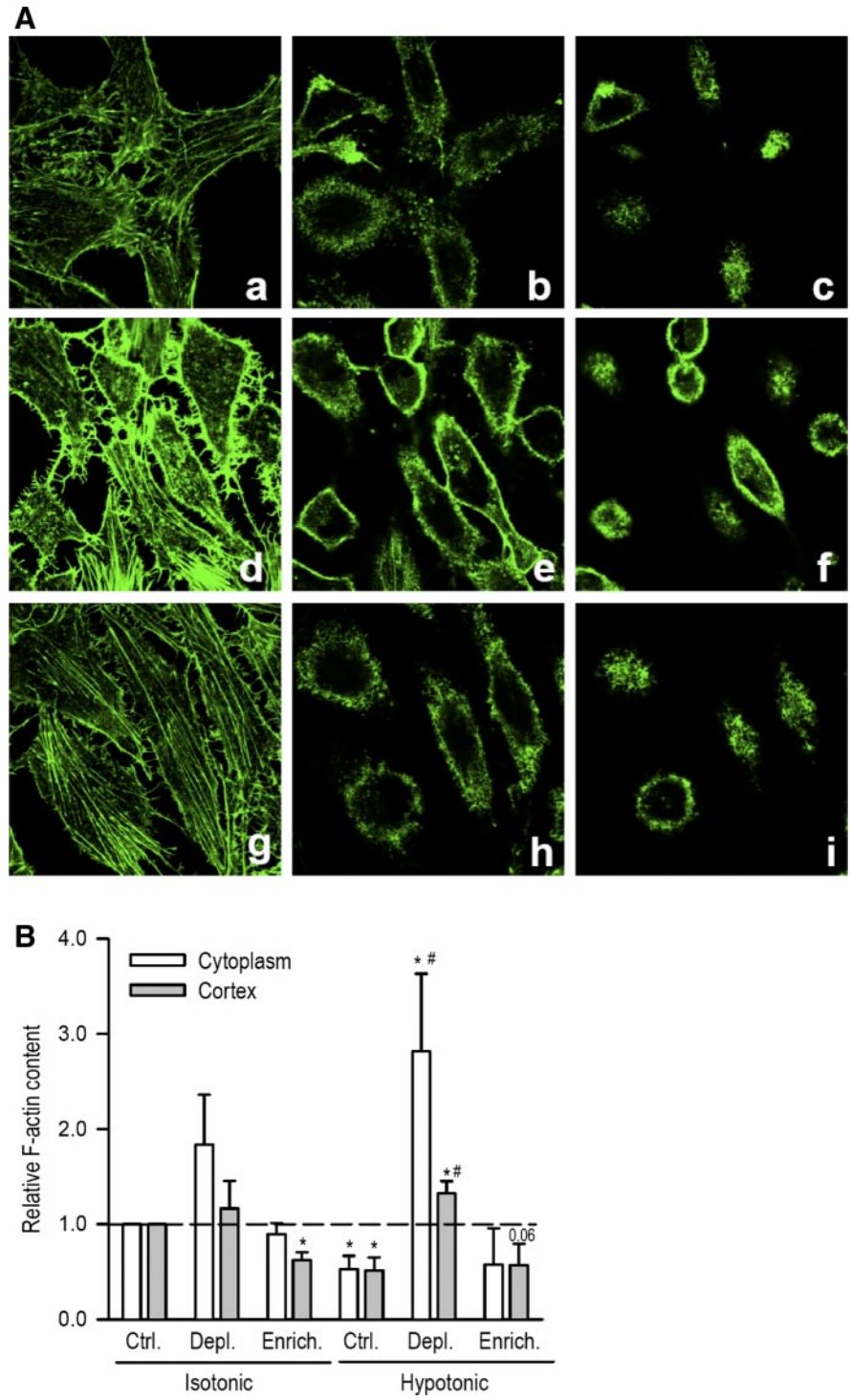

Fig. 4. Effect of cholesterol enrichment and depletion on F-actin organization in ELA cells. Cellular cholesterol content was increased by ~47% or decreased by ~44% by incubation with methyl-β-cyclodextrin (MβCD) in the absence or presence of added cholesterol. Subsequently, the cells were incubated for 10 min in the same isotonic saline used for electrophysiological experiments, paraformaldehyde fixed, permeabilized, and F-actin was labeled using FITC-conjugated phalloidin (2 U/ml), and visualized by confocal laser-scanning microscopy (Leica DM IRB/E microscope, Leica TSC NT confocal laser scanning unit, 567 nm argon/krypton laser line, ×40/1.25 numerical aperture planapochromat objective). *A*, *a–c*: control cells; *d–f*, cholesterol depleted; *g–i*, cholesterol-enriched. Images shown are frame-averaged 1 μm optical slices through the bottom (*a*, *d*, and *g*), middle (*b*, *e*, *h*), and top (*c*, *f*, *i*) of the cells. For details, see MATERIALS AND METHODS. The images shown are representative of findings in 5 independent experiments for each condition. Similar results were obtained in the standard isotonic saline ($n = 3$ and $n = 6$ for cholesterol enrichment and depletion, respectively, data not shown). *B*: quantification of pixel intensities. Experimental conditions were as in *A*, except that where indicated, cells were exposed to hypotonic conditions (255 mosmol/l) for 2 min. For each experiment, FITC-phalloidin intensities were quantified by defining regions of interest (ROI, of identical size in all experiments) in the cortical and cytoplasmic areas of several cells per slide, and determining the average pixel intensity in each ROI. Data are normalized to the value of isotonic control cells and are shown as mean ± SE bars. The number of independent experiments was 5 (control) and 4 (all other conditions). *#Value is significantly different from, respectively, the isotonic control value and the hypotonic control value.

which stimulates stress fiber formation by activating the small G protein Rho (e.g., Ref. 18), significantly increased the VRAC current magnitude when present (1 U/ml) simultaneously with a modest hypotonic challenge (255 mosmol/l). Similar to cholesterol depletion, thrombin had no effect on VRAC after a more severe hypotonic challenge (190 mosmol/l) (Fig. 6).

Effect of hypotonicity and cholesterol depletion on Rho activity. Given the above results, in conjunction with the previous findings that Rho is sensitive to cell volume changes (11), and has been shown by us and others to modulate VRAC (42, 47), we hypothesized that cholesterol depletion might alter VRAC currents by affecting Rho activity, and we therefore evaluated Rho activity in the ELA cells using a Rho-GTP pull-down assay (Fig. 7). Rho activity is shown as the amount of active Rho protein relative to total Rho protein. As expected, Rho activity was increased by ~75% after a 3-min exposure to thrombin (1 U/ml). In contrast, Rho activity was decreased by ~50% and ~20% after a 3-min exposure to 190 or 255 mosmol/l hypotonic conditions, respectively. Importantly, in cholesterol depleted cells, Rho activ-

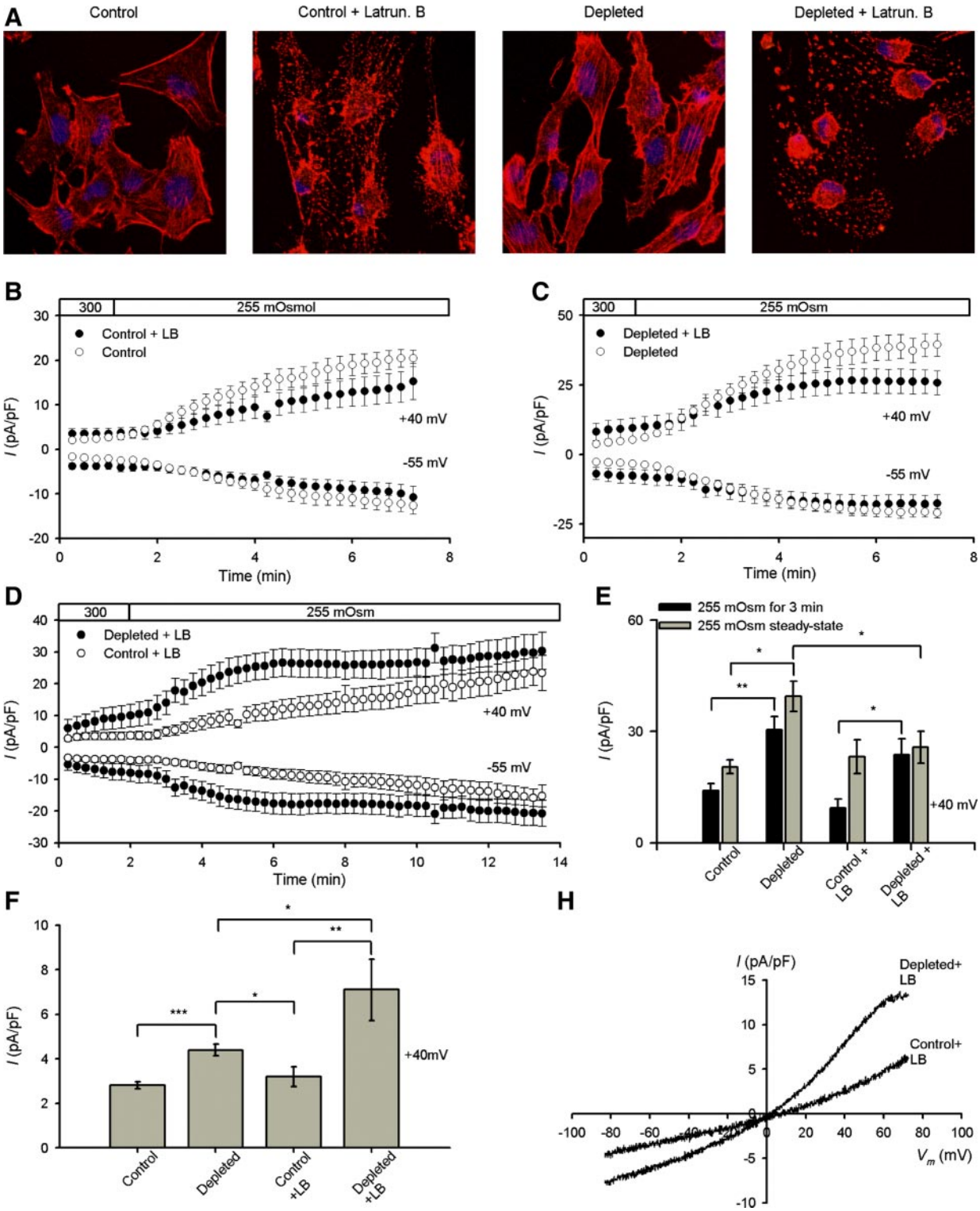

Fig. 5. Effect of latrunculin B on F-actin organization and volume-regulated anion current (VRAC) activation. *A*: ELA cells were incubated with 10 μM latrunculin B for 1 h (in cholesterol-depleted cells, this was done simultaneously to MβCD incubation). Cells were fixed and F-actin visualized as described in Fig. 3. Nuclei were visualized using 4,6-diamidino-2-phenylindole (DAPI) staining and the 364 nm UV laser line. Images are representative of three independent experiments for each set of conditions. *B–D*: VRAC as a function of time under isotonic conditions and after exposure to a 255 mosmol/l hypotonic challenge under control conditions and after LB pretreatment and/or cholesterol depletion as indicated. Current time points are obtained from 2.6-s fast voltage ramps from a holding potential of −40 mV, and are shown at +40 mV and −55 mV. *E*: data are calculated from the experiments shown in *B–D*, and are shown as means ± SE. *F*: mean current density at +40 mV, calculated in the first minute after obtaining stable whole cell conformations for cells incubated as indicated. *G*: representative *I/V* relationship for isotonic currents in LB-treated control and cholesterol-depleted cells. The number of independent experiments for each condition was 6 (control), 7 (depletion), 6 (control + LB), and 6 (depletion + LB), respectively. $*P < 0.05$, $**P < 0.01$, and $***P < 0.001$, significant differences calculated by independent *t*-tests.

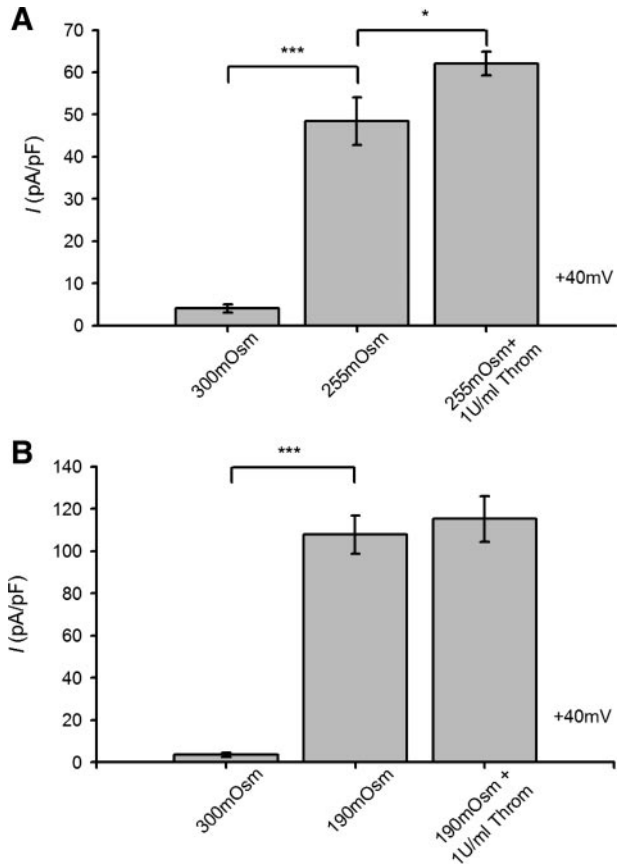

Fig. 6. Effect of thrombin on swelling-activated VRAC currents in ELA cells. Anion currents were measured using the fast ramp protocol described in Fig. 1. *A*: steady-state anion currents measured under isotonic (300 mosmol/l) and hypotonic (255 mosmol/l) conditions. After currents reached a steady-state hypotonic level cells were exposed to 255 mosmol/l hypotonic solution containing 1 U/ml thrombin, and currents were measured after 3-min exposure to thrombin ($n = 4$). To avoid Ca^{2+}-activated currents due to thrombin stimulation, $CaCl_2$ was excluded from the bath solution in these experiments. *B*: as in *A*, except that the osmolarity of the bath solution was 190 mosmol/l. $*P < 0.05$, $***P < 0.0001$.

ity was significantly increased under isotonic conditions, and the decrease in Rho activity after 255 mosmol/l, yet not after 190 mosmol/l hypotonic conditions, was abolished.

Effect of Rho kinase inhibitor Y27632 on VRAC. The Rho-Rho kinase pathway is a major regulator of F-actin organization, and we and others have implicated this pathway in VRAC regulation (42, 47). The maximal current magnitude after hypotonic swelling is similar in control cells and in cells treated with Y27632 to inhibit Rho kinase (Fig. 8, *A* and *B*). However, the rate of VRAC activation is reduced by Y27632 treatment. As seen in Fig. 8, *A* and *B*, a current significantly greater than the isotonic current value develops after 0.75 min in control cells exposed to a 15% hypotonic challenge, yet only after 2.25 min in Y27632-treated cells. An essentially similar pattern was seen in cholesterol-depleted cells (Fig. 8, *C* and *D*). Thus, under hypotonic conditions, Rho kinase activity appears to have a stimulatory effect on the rate of VRAC activation, whereas the maximal VRAC magnitude is unaffected. In congruence with this notion, the initial current activation rate (calculated by linear regression analysis of the current 15 to 90 s after hypotonic challenge) after exposure to a 15% hypotonic challenge was decreased nearly 2.5-fold by Y27632 treatment [4.78 ± 0.79 pA pF^{-1} min^{-1} ($n = 7$) in control cells, vs. 1.85 ± 1.18 pA pF^{-1} min^{-1} ($n = 6$) in Y27632-treated control cells, $P = 0.0585$]. Similarly, in cholesterol-depleted cells, the initial current activation rate was numerically decreased ~2-fold by Y27632 treatment, from 10.31 ± 1.86 pA pF^{-1} min^{-1} ($n = 7$) to 5.96 ± 2.08 pA pF^{-1} min^{-1} ($n = 6$) in Y27632-treated depleted cells ($P = 0.146$). Rho kinase inhibition had no effect on the isotonic current magnitude, neither in control cells nor after cholesterol depletion, and did not affect the cholesterol-induced increase in VRAC (Fig. 8, *E–G*).

Role of PtdIns(4,5)P_2 in modulation of VRAC. PtdIns(4,5)P_2 has been implicated in the effects of cholesterol depletion on F-actin, and we therefore evaluated the possible involvement of PtdIns(4,5)P_2 in VRAC activation. Inclusion of either 10 or 20 μM of the water soluble PtdIns(4,5)P_2 analog PtdIns(4,5)P_2 1,2 dioctanoyl in the patch pipette had no detectable effect on VRAC current density [the steady-state current density after osmotic swelling was 25.95 ± 4.00 pA pF^{-1} ($n = 6$) in control cells and 20.78 ± 2.52 pA pF^{-1} ($n = 7$) with 10 μM PtdIns(4,5)P_2 1,2 dioctanoyl, respectively]. Inclusion of a blocking PtdIns(4,5)P_2 antibody in the pipette to conversely reduce the amount of available PtdIns(4,5)P_2 was also without effect on VRAC activity [the steady-state current density after osmotic swelling was 23.35 ± 10.86 pA pF^{-1} ($n = 6$) under control conditions and 26.13 ± 7.20 pA pF^{-1} ($n = 7$) in the antibody-treated cells]. Finally, preincubation of the cells with neomycin to sequester PtdIns(4,5)P_2 failed to affect VRAC activity [the steady-state current density after osmotic swelling was 23.44 ± 3.35 pA pF^{-1} ($n = 8$) under control conditions and 18.39 ± 3.39 pA pF^{-1} ($n = 8$) after neomycin treatment]. To ascertain that the lack of effect of PtdIns(4,5)P_2 manipulation was not an experimental problem reflecting, e.g., poor solubility of PtdIns(4,5)P_2 dioctanoyl, we tested the effect of this compound on the transient receptor potential channel, TRPM4. Several TRPM channels are stimulated by PtdIns(4,5)P_2 (51), and PtdIns(4,5)P_2 has specifically been shown to rescue TRPM4 from desensitization (71). Inclusion of the PtdIns(4,5)P_2 analog (10 μM) in the pipette abolished TRPM4 desensitization as expected for this current [the current density at *time 5.5* min after activation of TRPM4 by 0.5 μM Ca^{2+} via the pipette was 1.84 ± 0.21 pA pF^{-1} ($n = 3$) under control conditions and 17.95 ± 5.51 pA pF^{-1} ($n = 3$) with 10 μM PtdIns(4,5)P_2 1,2 dioctanoyl in pipette solution]. It may also be noted that the same neomycin treatment dramatically affects phosphorylation of ezrin/radixin/moesin proteins in ELA cells (S. F. Pedersen, unpublished observations), suggesting that the lack of effect on VRAC is not due to, e.g., poor incorporation of the drug into ELA cells. Thus our findings indicate that neither increases nor decreases in the cellular PtdIns(4,5)P_2 level detectably affect VRAC in ELA cells, arguing against a role of this phospholipid in regulation of the current.

DISCUSSION

The VRAC current in ELA cells was activated in a dose-dependent manner by a reduction in extracellular osmolarity, was outwardly rectifying, exhibited slight time-dependent inactivation at depolarized potentials, and was inhibited by NPPB and DIDS, the latter in a voltage-dependent manner. The permeation sequence was $SCN^- > I^- > Br^- > Cl^- > Asp^-$,

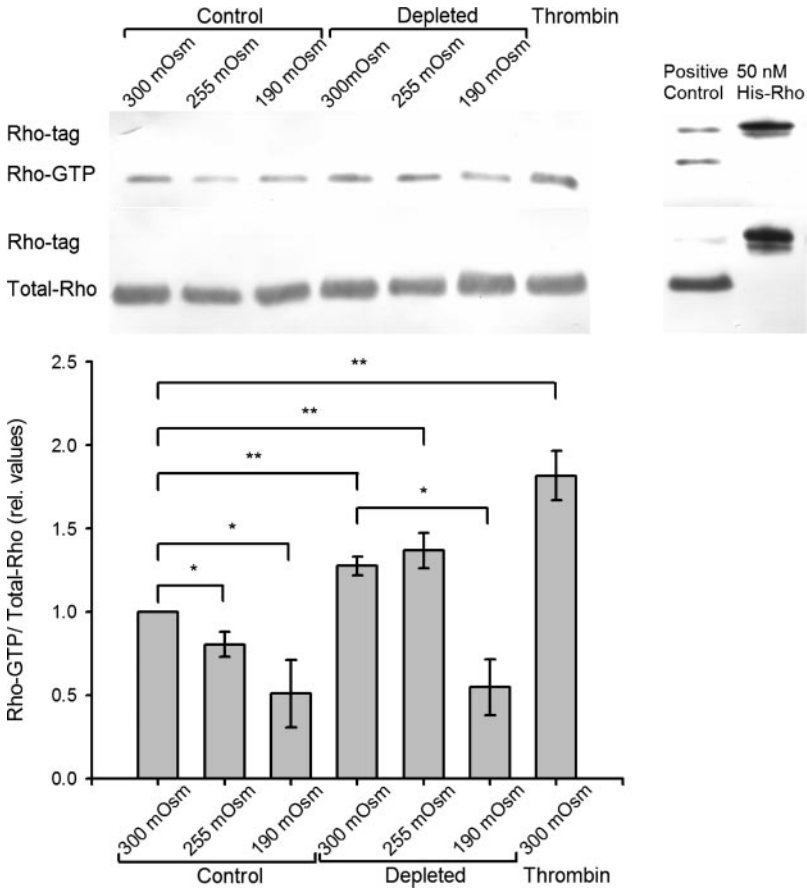

Fig. 7. Effect of hypotonic swelling on Rho activity in control cells and cholesterol-depleted cells. Confluent ELA cells in 10 cm petri dishes were cholesterol modulated as previously described and hereafter exposed to Ringer solutions of the osmolarities indicated for 3 min. Where indicated, thrombin was present for 3 min at 1 U/ml. The GTP-bound Rho in each sample was collected using a GST-RBD pull-down assay, as described in MATERIALS AND METHODS. The amount of precipitated GTP-Rho as well as total Rho was detected by SDS-PAGE and Western blot analysis using a monoclonal Rho antibody. *A*: typical experiment showing the purified GTP bound Rho (*top*) and total Rho (*bottom*). As a positive control for the pull-down assay, ELA cells were transfected with with Myc-tagged constitutively active Rho (RhoQ63L). To verify the specificity of the antibody, one lane was loaded with 50 nM purified His-tagged Rho. *B*: band intensity was quantified densitometrically. Rho-GTP band intensity values were normalized to the corresponding total Rho band intensity values, and are given relative to the value in the isotonic control (n = 3–4). *$P < 0.05$ and **$P < 0.01$, significant difference.

consistent with an Eisenman I profile. P_x/P_{Cl} correlated inversely with the Jones-Dole viscosity B coefficient, indicating a reverse correlation between hydration energy and permeability for smaller anions (12, 54, 55). This is indicative of low-energy interactions between ion and channel as also indicated by the Eisenman I sequence (68), and indicates that although VRAC is seemingly a water-permeable channel (39), it is not a simple pore for hydrated ions. Thus VRAC in ELA cells exhibits biophysical and pharmacological characteristics similar to those reported in other cell types (see Refs. 40, 44, 52).

A 44% reduction in cellular cholesterol content resulted in a significant potentiation of VRAC in ELA cells after mild (255 mosmol/l), but not after severe (190 osmol/l), hypotonic stress, in accordance with findings in BAE cells (30). Levitan and coworkers (30) also pointed out the fact that cholesterol depletion activates VRAC only after mild osmotic stress is consistent with a cholesterol-depletion induced increase in the fraction of open channels, rather than an effect on single channel conductance, a notion supported by observation of single-channel events (56). In contrast, an increase in cellular cholesterol content of ~47% had no detectable effect on VRAC in ELA cells, in apparent contrast to findings in BAE cells (30). This difference is not due to insufficient cholesterol enrichment in ELA cells because the relative cholesterol enrichment was in fact greater than that in the BAE cells (30). More likely, it reflects that the effect of cholesterol on VRAC is already maximal in ELA cells at the normal cellular cholesterol content and under the osmotic conditions tested. Absolute membrane cholesterol levels under control, depleted, and enriched conditions were similar in ELA and BAE cells; hence, other differences in membrane/cortical structure and/or VRAC sensitivity to cholesterol in the two cell types appear likely. In congruence with this, cell type-specific effects of cholesterol were reported for the Na^+/H^+ exchanger, NHE1 (16). Notably, NHE1, which is a shrinkage-activated transporter, was activated by cholesterol enrichment (16), i.e., an effect of cholesterol opposite to that on VRAC. In conjunction with the finding that cholesterol depletion activated a VRAC-like current in ELA (the present study) and BAE cells (56) also in the absence of cell swelling, this might suggest that changes in cholesterol content affect the volume signal per se or some component necessary for its transduction, and hereby increases the fraction of open VRAC channels. Clearly, changes in cholesterol content are not the volume signal per se: so, what might this putative volume- and cholesterol-sensitive parameter be? It is unlikely to be membrane thickness, which, as estimated from membrane capacitance, is not generally altered by cell swelling (see Ref. 49), a notion confirmed in ELA cells (A. Bergdahl, T. Kjær Klausen, and E. K. Hoffmann, unpublished observations). Cholesterol depletion/enrichment had no detectable effect on membrane capacitance in ELA cells (control cells 36 ± 2.4 pF, n = 21; depleted 36 ± 3.5 pF, n = 13; enriched 31 ± 1.9 pF; n = 14), similar to findings in BAE cells (30). A putative volume- and cholesterol-sensitive parameter could be membrane deformability or stiffness, which is dependent on cortical F-actin. Cholesterol depletion completely abolished the swelling-induced decrease in cortical and stress fiber-

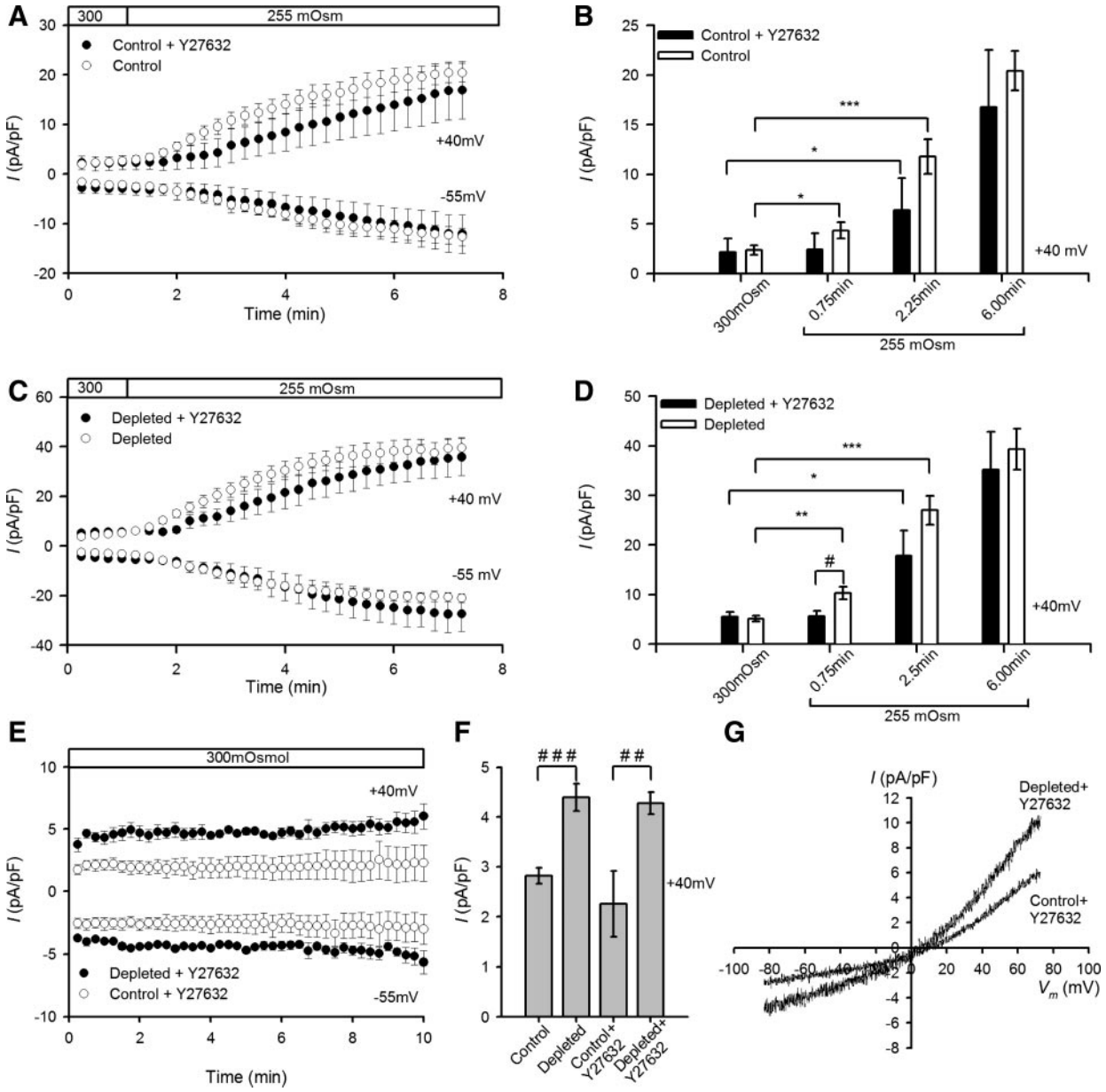

Fig. 8. Effect of the Rho kinase inhibitor Y27632 on VRAC. *A*: VRAC development as a function of time under isotonic conditions and after exposure to a 255 mosmol/l hypotonic challenge. Current time points at +40 and −55 mV were calculated from the traces obtained using 2.6-s voltage ramps. Where indicated, the Rho kinase inhibitor Y27623 was present in the bath at a concentration of 10 μM. *B*: summary data calculated from the experiments shown in *A*. Current magnitude at +40 mV was calculated under isotonic conditions (300 mosmol/l) and at times 0.75, 2.25, and 6 min. *C* and *D*: as in *A* and *B*, except that cells were cholesterol depleted using MβCD, as described in MATERIALS AND METHODS. The number of independent experiments were 6 (ctrl.), 6 (Y27632), 7 (chol. depl.), and 5 (chol. depl.Y27632), respectively. *E*: before hypotonic stimulation, the cells were maintained in the whole cell configuration for 10 min with 10 μM Y27632 constantly present in the isotonic bath solution. Currents in this time interval was measured as in *A* and currents measured at membrane potentials −55 and +40 mV are shown. *F*: mean current density at +40 mV was calculated during the first minute after obtaining stable whole cell conformations. *G*: representative *I/V* relationship for isotonic currents in Y27632-treated control and cholesterol-depleted cells. $^{*}P < 0.05$, $^{**}P < 0.01$, and $^{***}P < 0.001$, significant differences, all in paired *t*-tests. #$P < 0.05$, ##$P < 0.01$, and ###$P < 0.001$, significant difference in independent *t*-tests.

associated F-actin in ELA cells, consistent with the view that cell stiffness is increased. Whereas in isolated lipid bilayers, cholesterol depletion is associated with a reduction in stiffness and deformation energy (e.g., Refs. 32 and 37), it appears that the presence of a cortical cytoskeleton may result in the opposite effect on the total elastic properties of the membrane. Thus, in BAE cells, cholesterol depletion was associated with an increase in membrane stiffness which was abolished upon disruption of F-actin by latrunculin A (6). Similarly, in sperm cells, cholesterol depletion was associated with an increase in F-actin content (3). In human skin fibroblasts, cholesterol depletion elicited a more complex F-actin reorganization, including an apparent decrease in stress fiber content, increase in cortical F-actin content, and increased F-actin turnover (27).

Cell swelling is generally associated with F-actin depolymerization, whereas the converse is true for cell shrinkage (see Ref. 49). In ELA cells, the isotonic VRAC current induced by cholesterol depletion was strongly potentiated by F-actin dis-

ruption by LB, whereas after cell swelling, LB prevented the cholesterol depletion-induced increase in maximal current magnitude, yet not the cholesterol depletion-induced increase in VRAC activation rate. Taken together, it appears that in ELA cells, F-actin integrity and/or an increase in F-actin is required on the one hand for limiting isotonic VRAC activity in cholesterol-depleted cells, and on the other hand for the cholesterol-depletion-induced increase in VRAC magnitude under hypotonic conditions. Such a scenario would resemble the regulation of the Na^+-K^+-$2Cl^-$ cotransporter NKCC1 by hypertonic shrinkage and F-actin, which appears to be such that F-actin integrity is required both to maintain NKCC1 silent under isotonic steady-state conditions, and for its shrinkage-induced activation (see Ref. 49). Moreover, the differential effects of F-actin disruption on VRAC maximal current and activation rate, respectively, indicate that there are at least two components in the potentiation of VRAC by cholesterol depletion, one F-actin dependent and the other F-actin independent.

The mechanism(s) of regulation of VRAC by F-actin in cholesterol-depleted cells remains to be elucidated. Cholesterol depletion-induced reinforcement of cortical and stress-fiber associated F-actin might somehow facilitate volume sensing, maybe due to a dependence on the overall cytoskeletal tension in the cell, as reported for mechanosensing (e.g., Ref. 1). In apparent contrast to our findings and those of Levitan and co-workers, potentiation of hypotonic VRAC currents by cytochalasin D has been observed in human epithelial cells, and proposed to reflect modulation of VRAC by the F-actin-dependent membrane spring energy (35) and/or augmentation of VRAC activity by membrane unfolding (44). It would appear that at least two opposing effects of F-actin may be working on VRAC, and that their relative roles may differ between cell types, resulting in different net effects of F-actin disrupting agents: *1*) an "unfolding" effect, by which F-actin depolymerization (here induced by swelling or by LB) potentiates VRAC, and *2*) a potentiation of volume sensing, by which F-actin polymerization (here induced by cholesterol depletion) conversely potentiates VRAC. While not directly addressed here, it should also be kept in mind that different cellular F-actin pools (cortical, stress fiber associated, etc.) may be involved in the various effects of F-actin on VRAC. Further experiments are required to address this, and to verify whether the apparently contradictory findings reflect cell type specific effects or differences in experimental protocols. With respect to the latter it may be noted that high concentrations of cytochalasin D (>1 μM), compared with 5 μM as used in (35) can in fact increase, rather than decrease, actin polymerization (15).

PtdIns(4,5)P_2 is a major regulator of F-actin organization, and cholesterol depletion was found to reduce PtdIns(4,5)P_2 levels in the plasma membrane (27). Moreover, cell swelling is generally, and also in EAT cells, associated with decreased PtdIns(4,5)P_2 levels while the converse is true for cell shrinkage (see Ref. 49). However, neither increasing [using the water-soluble PtdIns(4,5)P_2 analog PtdIns(4,5)P_2 1,2-dioctanoyl] nor decreasing [using neomycin sequestering or PtdIns(4,5)P_2 blocking antibodies] the cellular PtdIns(4,5)P_2 level had any detectable effect on VRAC activation in ELA cells, whereas a positive control experiment showed substantial effect of PtdIns(4,5)P_2 dioctanoyl on TRPM4 in the same cells. Thus, while such a role of course cannot be unequivocally excluded based on negative findings, the results obtained in the present study do not support a role for PtdIns(4,5)P_2 in regulation of VRAC.

Rho family G proteins and their effectors are major regulators of F-actin organization, and their activity has been shown to be increased by cell shrinkage (11). Consistent with this, Rho activity was dose-dependently attenuated by ELA cell swelling. Notably, cholesterol depletion increased isotonic Rho activity and prevented the swelling-induced attenuation of Rho activity after mild hypotonic exposure (255 mosmol/l). The fact that thrombin, which activates Rho and promotes F-actin polymerization, stimulates VRAC (Fig. 6), is consistent with potentiation of VRAC by Rho activity and F-actin polymerization. If this is so, one would expect that under normal conditions, swelling-induced Rho inhibition and F-actin depolymerization tend to attenuate VRAC activity, and hence, that cholesterol depletion may increase the maximal VRAC current (which was inhibited by LB, i.e., F-actin dependent, but unaffected by Y27632, i.e., not Rho kinase dependent), and the rate of VRAC activation (which was Rho kinase but not F-actin dependent) by increasing Rho activity and causing actin polymerization. These findings are in good agreement with previous reports by us and others showing that while the Rho-ROK pathway is not the volume-sensing mechanism per se, it has a potentiating effect on swelling-induced VRAC activity (7, 41, 42, 47). In contrast to the hypotonic VRAC current, the isotonic current, which was also stimulated by cholesterol depletion, was potentiated by F-actin disruption and unaffected by Rho kinase inhibition. This may indicate that the mechanism of stimulation by cholesterol depletion may be at least partially different between these two conditions.

The mechanism by which cholesterol depletion affects Rho activity remains to be determined. RhoA and Rho kinase exhibit activity-dependent translocation to caveolae (62, 65), suggesting a role for cholesterol depletion-induced changes in caveolae organization. Interestingly, caveolae are also sensitive to cell volume perturbations (46), and have been implicated in VRAC regulation (63, 64). On the other hand, preliminary studies revealed no detectable changes in caveolin-1 distribution in cholesterol-depleted ELA cells (S. F. Pedersen, T. Kjær Klausen, and E. K. Hoffmann, unpublished observations). Thus further studies are required to determine the relative roles in the cholesterol-depletion-induced effects on VRAC of the following: *1*) changes in membrane stiffness resulting from cytoskeletal reorganization, *2*) effects on Rho signaling, and *3*) caveolar reorganization.

In conclusion, in ELA cells, cholesterol depletion increased VRAC activation rate and maximal current after a modest (15%), but not after a severe (36%) reduction in extracellular osmolarity. The cholesterol depletion-induced increase in maximal VRAC current and activation rate were dependent on F-actin and ROK, respectively, whereas changes in cellular PtdIns(4,5)P_2 had no effect on VRAC. Rho activity was decreased in osmotically swollen cells, and this reduction was prevented by cholesterol depletion, which also increased Rho activity under isotonic conditions. It is suggested that in ELA cells, F-actin, and the Rho-Rho kinase pathway modulate VRAC activity, and that cholesterol depletion increases VRAC currents at least in part by preventing the hypotonicity-induced decrease in Rho activity and promoting F-actin polymerization.

ACKNOWLEDGMENTS

We are indebted to Dr. Andreas Bergdahl for performing the experiments demonstrating the effect of PtdIns(4,5)P_2 on TRPM4. We also gratefully acknowledge Dr. Claus Helix Nielsen (Quantum Protein Centre, Technical University of Denmark), and Robert Nielsen and Susanne Larsen (Institute of Molecular Biology and Physiology, University of Copenhagen) for stimulating discussions. Finally, we express our gratitude to Dr. Andras Kapus (St. Michael's Hospital, Toronto, ONT, Canada) for kindly providing the RhoQ63L construct.

GRANTS

The study was supported by the Danish Natural Sciences Research Foundation Grants 21-01-0507 and 21-04-0535 (to E. K. Hoffmann and S. F. Pedersen) and the Carlsberg Foundation (to C. Hougaard and E. K. Hoffmann).

REFERENCES

1. **Alenghat FJ, Nauli SM, Kolb R, Zhou J, and Ingber DE.** Global cytoskeletal control of mechanotransduction in kidney epithelial cells. *Exp Cell Res* 301: 23–30, 2004.
2. **Arbuzova A, Martushova K, Hangyas-Mihalyne G, Morris AJ, Ozaki S, Prestwich GD, and McLaughlin S.** Fluorescently labeled neomycin as a probe of phosphatidylinositol-4,5-bisphosphate in membranes. *Biochim Biophys Acta* 1464: 35–48, 2000.
3. **Brener E, Rubinstein S, Cohen G, Shternall K, Rivlin J, and Breitbart H.** Remodeling of the actin cytoskeleton during mammalian sperm capacitation and acrosome reaction. *Biol Reprod* 68: 837–845, 2003.
4. **Brown DA and London E.** Structure and function of sphingolipid- and cholesterol-rich membrane rafts. *J Biol Chem* 275: 17221–17224, 2000.
5. **Burger K, Gimpl G, and Fahrenholz F.** Regulation of receptor function by cholesterol. *Cell Mol Life Sci* 57: 1577–1592, 2000.
6. **Byfield FJ, Aranda-Espinoza H, Romanenko VG, Rothblat GH, and Levitan I.** Cholesterol depletion increases membrane stiffness of aortic endothelial cells. *Biophys J* 87: 3336–3343, 2004.
7. **Carton I, Trouet D, Hermans D, Barth H, Aktories K, Droogmans G, Jorgensen NK, Hoffmann EK, Nilius B, and Eggermont J.** RhoA exerts a permissive effect on volume-regulated anion channels in vascular endothelial cells. *Am J Physiol Cell Physiol* 283: C115–C125, 2002.
8. **Chen M, Mason RP, and Tulenko TN.** Atherosclerosis alters the composition, structure and function of arterial smooth muscle cell plasma membranes. *Biochim Biophys Acta* 1272: 101–112, 1995.
9. **Christensen O and Hoffmann EK.** Cell swelling activates K^+ and Cl^- channels as well as nonselective, stretch-activated cation channels in Ehrlich ascites tumor cells. *J Membr Biol* 129: 13–36, 1992.
10. **Christian AE, Haynes MP, Phillips MC, and Rothblat GH.** Use of cyclodextrins for manipulating cellular cholesterol content. *J Lipid Res* 38: 2264–2272, 1997.
11. **Ciano-Oliveira C, Sirokmany G, Szaszi K, Arthur WT, Masszi A, Peterson M, Rotstein OD, and Kapus A.** Hyperosmotic stress activates Rho: differential involvement in Rho kinase-dependent MLC phosphorylation and NKCC activation. *Am J Physiol Cell Physiol* 285: C555–C566, 2003.
12. **Collins KD.** Ions from the Hofmeister series and osmolytes: effects on proteins in solution and in the crystallization process. *Methods* 34: 300–311, 2004.
13. **Di Ciano C, Nie Z, Szaszi K, Lewis A, Uruno T, Zhan X, Rotstein OD, Mak A, and Kapus A.** Osmotic stress-induced remodeling of the cortical cytoskeleton. *Am J Physiol Cell Physiol* 283: C850–C865, 2002.
14. **Estevez AY, Bond T, and Strange K.** Regulation of $I_{Cl,swell}$ in neuroblastoma cells by G protein signaling pathways. *Am J Physiol Cell Physiol* 281: C89–C98, 2001.
15. **Franki N, Ding G, Gao Y, and Hays RM.** Effect of cytochalasin D on the actin cytoskeleton of the toad bladder epithelial cell. *Am J Physiol Cell Physiol* 263: C995–C1000, 1992.
16. **Fuster D, Moe OW, and Hilgemann DW.** Lipid- and mechanosensitivities of sodium/hydrogen exchangers analyzed by electrical methods. *Proc Natl Acad Sci USA* 101: 10482–10487, 2004.
17. **Gimpl G, Burger K, and Fahrenholz F.** Cholesterol as modulator of receptor function. *Biochemistry* 36: 10959–10974, 1997.
18. **Gohla A, Offermanns S, Wilkie TM, and Schultz G.** Differential involvement of Gα12 and Gα13 in receptor-mediated stress fiber formation. *J Biol Chem* 274: 17901–17907, 1999.
19. **Hajdu P, Varga Z, Pieri C, Panyi G, and Gaspar R Jr.** Cholesterol modifies the gating of Kv1.3 in human T lymphocytes. *Pflügers Arch* 445: 674–682, 2003.
20. **Hallows KR, Packman CH, and Knauf PA.** Acute cell volume changes in anisotonic media affect F-actin content of HL-60 cells. *Am J Physiol Cell Physiol* 261: C1154–C1161, 1991.
21. **Harder T, Kellner R, Parton RG, and Gruenberg J.** Specific release of membrane-bound annexin II and cortical cytoskeletal elements by sequestration of membrane cholesterol. *Mol Biol Cell* 8: 533–545, 1997.
22. **Harder T and Simons K.** Clusters of glycolipid and glycosylphosphatidylinositol-anchored proteins in lymphoid cells: accumulation of actin regulated by local tyrosine phosphorylation. *Eur J Immunol* 29: 556–562, 1999.
23. **Hoffmann EK.** Regulation of cell volume by selective changes in the leak permeabilities of Ehrlich ascites tumor cells. *Alfred Benzon Symposium* XI: 397–417, 1978.
24. **Hoffmann EK and Dunham PB.** Membrane mechanisms and intracellular signalling in cell volume regulation. *Int Rev Cytol* 161: 173–262, 1995.
25. **Huang HW.** Deformation free energy of bilayer membrane and its effect on gramicidin channel lifetime. *Biophys J* 50: 1061–1070, 1986.
26. **Jorgensen NK, Pedersen SF, Rasmussen HB, Grunnet M, Klaerke DA, and Olesen SP.** Cell swelling activates cloned Ca^{2+}-activated K^+ channels: a role for the F-actin cytoskeleton. *Biochim Biophys Acta* 1615: 115–125, 2003.
27. **Kwik J, Boyle S, Fooksman D, Margolis L, Sheetz MP, and Edidin M.** Membrane cholesterol, lateral mobility, and the phosphatidylinositol 4,5-bisphosphate-dependent organization of cell actin. *Proc Natl Acad Sci USA* 100: 13964–13969, 2003.
28. **Laux T, Fukami K, Thelen M, Golub T, Frey D, and Caroni P.** GAP43, MARCKS, and CAP23 modulate PI(4,5)P_2 at plasmalemmal rafts, and regulate cell cortex actin dynamics through a common mechanism. *J Cell Biol* 149: 1455–1472, 2000.
29. **Levitan I, Almonte C, Mollard P, and Garber SS.** Modulation of a volume-regulated chloride current by F-actin. *J Membr Biol* 147: 283–294, 1995.
30. **Levitan I, Christian AE, Tulenko TN, and Rothblat GH.** Membrane cholesterol content modulates activation of volume-regulated anion current in bovine endothelial cells. *J Gen Physiol* 115: 405–416, 2000.
31. **Lundbaek JA and Andersen OS.** Spring constants for channel-induced lipid bilayer deformations. Estimates using gramicidin channels. *Biophys J* 76: 889–895, 1999.
32. **Lundbaek JA, Birn P, Hansen AJ, Sogaard R, Nielsen C, Girshman J, Bruno MJ, Tape SE, Egebjerg J, Greathouse DV, Mattice GL, Koeppe RE, and Andersen OS.** Regulation of sodium channel function by bilayer elasticity: the importance of hydrophobic coupling. Effects of Micelle-forming amphiphiles and cholesterol. *J Gen Physiol* 123: 599–621, 2004.
33. **McCloskey HM, Rothblat GH, and Glick JM.** Incubation of acetylated low-density lipoprotein with cholesterol-rich dispersions enhances cholesterol uptake by macrophages. *Biochim Biophys Acta* 921: 320–332, 1987.
34. **Mills JW, Falsig PS, Walmod PS, and Hoffmann EK.** Effect of cytochalasins on F-actin and morphology of Ehrlich ascites tumor cells. *Exp Cell Res* 261: 209–219, 2000.
35. **Morishima S, Shimizu T, Kida H, and Okada Y.** Volume expansion sensitivity of swelling-activated Cl^- channel in human epithelial cells. *Jpn J Physiol* 50: 277–280, 2000.
36. **Nebl T, Pestonjamasp KN, Leszyk JD, Crowley JL, Oh SW, and Luna EJ.** Proteomic analysis of a detergent-resistant membrane skeleton from neutrophil plasma membranes. *J Biol Chem* 277: 43399–43409, 2002.
37. **Needham D and Nunn RS.** Elastic deformation and failure of lipid bilayer membranes containing cholesterol. *Biophys J* 58: 997–1009, 1990.
38. **Nielsen C, Goulian M, and Andersen OS.** Energetics of inclusion-induced bilayer deformations. *Biophys J* 74: 1966–1983, 1998.
39. **Nilius B.** Is the volume-regulated anion channel VRAC a "water-permeable" channel? *Neurochem Res* 29: 3–8, 2004.
40. **Nilius B and Droogmans G.** Ion channels and their functional role in vascular endothelium. *Physiol Rev* 81: 1415–1459, 2001.
41. **Nilius B, Prenen J, Walsh MP, Carton I, Bollen M, Droogmans G, and Eggermont J.** Myosin light chain phosphorylation-dependent modulation of volume-regulated anion channels in macrovascular endothelium. *FEBS Lett* 466: 346–350, 2000.
42. **Nilius B, Voets T, Prenen J, Barth H, Aktories K, Kaibuchi K, Droogmans G, and Eggermont J.** Role of Rho and Rho kinase in the

activation of volume-regulated anion channels in bovine endothelial cells. *J Physiol* 516: 67–74, 1999.
43. **Oike M, Schwarz G, Sehrer J, Jost M, Gerke V, Weber K, Droogmans G, and Nilius B.** Cytoskeletal modulation of the response to mechanical stimulation in human vascular endothelial cells. *Pflügers Arch* 428: 569–576, 1994.
44. **Okada Y.** Volume expansion-sensing outward-rectifier Cl^- channel: fresh start to the molecular identity and volume sensor. *Am J Physiol Cell Physiol* 273: C755–C789, 1997.
45. **Okada Y, Maeno E, Shimizu T, Manabe K, Mori S, and Nabekura T.** Dual roles of plasmalemmal chloride channels in induction of cell death. *Pflügers Arch* 448: 287–295, 2004.
46. **Parton RG, Joggerst B, and Simons K.** Regulated internalization of caveolae. *J Cell Biol* 127: 1199–1215, 1994.
47. **Pedersen SF, Beisner KH, Hougaard C, Willumsen BM, Lambert IH, and Hoffmann EK.** Rho family GTP binding proteins are involved in the regulatory volume decrease process in NIH3T3 mouse fibroblasts. *J Physiol* 541: 779–796, 2002.
48. **Pedersen SF and Hoffmann EK.** Possible interrelationship between changes in F-actin and myosin II, protein phosphorylation, and cell volume regulation in Ehrlich ascites tumor cells. *Exp Cell Res* 277: 57–73, 2002.
49. **Pedersen SF, Hoffmann EK, and Mills JW.** The cytoskeleton and cell volume regulation. *Comp Biochem Physiol A* 130: 385–399, 2001.
50. **Pedersen SF, Mills JW, and Hoffmann EK.** Role of the F-actin cytoskeleton in the RVD and RVI processes in Ehrlich ascites tumor cells. *Exp Cell Res* 252: 63–74, 1999.
51. **Pedersen SF, Owsianik G, and BTRP.** Nilius channels: an overview. *Cell Calcium* 38: 233–252, 2005.
52. **Pedersen SF, Prenen J, Droogmans G, Hoffmann EK, and Nilius B.** Separate swelling- and Ca^{2+}-activated anion currents in Ehrlich ascites tumor cells. *J Membr Biol* 163: 97–110, 1998.
53. **Riquelme G, Sepulveda FV, Jorgensen F, Pedersen S, and Hoffmann EK.** Swelling-activated potassium currents of Ehrlich ascites tumour cells. *Biochim Biophys Acta* 1371: 101–106, 1998.
54. **Robinson JB Jr, Strottmann JM and Stellwagen E.** Prediction of neutral salt elution profiles for affinity chromatography. *Proc Natl Acad Sci USA* 78: 2287–2291, 1981.
55. **Robinson RA and Stokes RH.** The measurement and interpretation of conductance, chemical potentials and diffusion of solutions of simple electrolytes. In: *Electrolyte Solutions* (2nd ed.). London: Butterworths, 1959.
56. **Romanenko VG, Rothblat GH, and Levitan I.** Sensitivity of volume-regulated anion current to cholesterol structural analogues. *J Gen Physiol* 123: 77–87, 2004.
57. **Rozelle AL, Machesky LM, Yamamoto M, Driessens MH, Insall RH, Roth MG, Luby-Phelps K, Marriott G, Hall A, and Yin HL.** Phosphatidylinositol 4,5-bisphosphate induces actin-based movement of raft-enriched vesicles through WASP-Arp2/3. *Curr Biol* 10: 311–320, 2000.
58. **Sabirov RZ, Prenen J, Tomita T, Droogmans G, and Nilius B.** Reduction of ionic strength activates single volume-regulated anion channels (VRAC) in endothelial cells. *Pflügers Arch* 439: 315–320, 2000.
59. **Simons K and Toomre D.** Lipid rafts and signal transduction. *Nat Rev Mol Cell Biol* 1: 31–39, 2000.
60. **Simons K and Vaz WL.** Model systems, lipid rafts, and cell membranes. *Annu Rev Biophys Biomol Struct* 33: 269–295, 2004.
61. **Stahlhut M and van Deurs B.** Identification of filamin as a novel ligand for caveolin-1: evidence for the organization of caveolin-1-associated membrane domains by the actin cytoskeleton. *Mol Biol Cell* 11: 325–337, 2000.
62. **Taggart MJ, Lee YH, and Morgan KG.** Cellular redistribution of PKCα, rhoA, and ROKα following smooth muscle agonist stimulation. *Exp Cell Res* 251: 92–101, 1999.
63. **Trouet D, Hermans D, Droogmans G, Nilius B, and Eggermont J.** Inhibition of volume-regulated anion channels by dominant-negative caveolin-1. *Biochem Biophys Res Commun* 284: 461–465, 2001.
64. **Trouet D, Nilius B, Jacobs A, Remacle C, Droogmans G, and Eggermont J.** Caveolin-1 modulates the activity of the volume-regulated chloride channel. *J Physiol* 520: 113–119, 1999.
65. **Urban NH, Berg KM, and Ratz PH.** K^+ depolarization induces RhoA kinase translocation to caveolae and Ca^{2+} sensitization of arterial muscle. *Am J Physiol Cell Physiol* 285: C1377–C1385, 2003.
66. **Voets T, Droogmans G, Raskin G, Eggermont J, and Nilius B.** Reduced intracellular ionic strength as the initial trigger for activation of endothelial volume-regulated anion channels. *Proc Natl Acad Sci USA* 96: 5298–5303, 1999.
67. **Westermann M, Steiniger F, and Richter W.** Belt-like localisation of caveolin in deep caveolae and its re-distribution after cholesterol depletion. *Histochem Cell Biol* 123: 613–620, 2005.
68. **Wright EM and Diamond JM.** Anion selectivity in biological systems. *Physiol Rev* 57: 109–156, 1977.
69. **Yeagle PL.** Cholesterol and the cell membrane. *Biochim Biophys Acta* 822: 267–287, 1985.
70. **Zhang J, Larsen TH, and Lieberman M.** F-actin modulates swelling-activated chloride current in cultured chick cardiac myocytes. *Am J Physiol Cell Physiol* 273: C1215–C1224, 1997.
71. **Zhang Z, Okawa H, Wang Y, and Liman ER.** Phosphatidylinositol 4,5-bisphosphate rescues TRPM4 channels from desensitization. *J Biol Chem* 280: 39185–39192, 2005.